


COMPUTATIONAL INSIGHTS INTO THE SPONTANEITY OF EPOXIDE FORMATION FROM HALOHYDRINS AND OTHER MECHANISTIC DETAILS OF WILLIAMSON'S ETHER SYNTHESIS

Pedro J. Silva 

FP-I3ID,FP-BHS / Faculdade de Ciências da Saúde, Universidade Fernando Pessoa,
296, Rua Carlos da Maia, 4200-150 Porto, Portugal
LAQV/REQUIMTE, BioSIM – Department of Biomedicine, Faculty of Medicine, University of Porto,
4200-319 Porto, Portugal
e-mail: pedro.dft@gmail.com

Abstract. The reaction mechanism of several Williamson's ether syntheses have been studied using density functional theory with triple- ζ basis sets. These computations show that the synthesis of geometrically-strained epoxide from deprotonated halohydrins is due to the combined effects of favourable solvation of the products, higher bond enthalpy of C-O bonds vs. C-Cl bonds and increased vibrational entropy of the epoxide vs. the original halohydrin. Examination of the pathways leading to the formation of larger cyclic ethers revealed that the experimentally-observed preference for the formation of five-atom rings over six-atom-rings is due to the preference of the intervening methylene groups for staggered conformations, which entails that the alkyl carbon in the reactant state leading to the six-atom cyclic ether is initially not properly aligned with the attacking alkoxide. Study of the competing elimination reactions further shows that during the synthesis of five-atom cyclic ethers the competing elimination reaction is strongly disfavoured due to steric effects. The temperature dependence of both reactions favours elimination over S_N2 as temperature rises, though only when the alkoxide and the halogen moieties are not part of the same carbon chain.

Keywords: density-functional theory, reaction mechanism, intra-molecular Williamson's ether synthesis, epoxide, halohydrin.

Received: 16 May 2023/ Revised final: 07 September 2023/ Accepted: 11 September 2023

Introduction

Many asymmetric ethers may be synthesized from haloalkanes and alcohols under alkaline conditions using the well-known Williamson's ether synthesis, which is basically an S_N2 reaction using an alkoxide as nucleophile and a halogen as a leaving group [1-3]. If the leaving group and the alcohol functional group are part of a single molecule, the reaction may also proceed intramolecularly, leading to the synthesis of cyclic ethers [4]. An especially striking example of such an intramolecular Williamson ether synthesis occurs when a halohydrin is deprotonated by a strong base, yielding an epoxide (Figure 1). Since epoxides suffer from considerable angular strain, this reaction might be expected, at first sight, to be thermodynamically disfavoured relative to the reverse reaction, in contrast to the experimental observations. This apparent contradiction has not been previously addressed quantitatively in the literature using state-of-the-art theoretical

methods. This communication describes a density-functional-theory exploration of the thermodynamics and kinetics of these reactions, and how the degree of substitution of the halogenated carbon or the distance of the halogenated carbon from the hydroxylated carbon influences their exergonicity and activation energies. The results show that the epoxide formation is enabled by the favourable contribution of leaving group solvation and by the increase of entropy afforded by halogen expulsion, and that the slower rate of formation of six-atom cyclic ethers vs. the five-atom cyclic ethers is governed by the preference of the intervening methylene groups for staggered conformations, which entails that the alkyl carbon in the reactant state leading to the six-atom cyclic ether is not properly aligned with the attacking alkoxide. The computations also identify the conditions where the competing elimination reaction may (or not) hinder the desired reaction outcome.

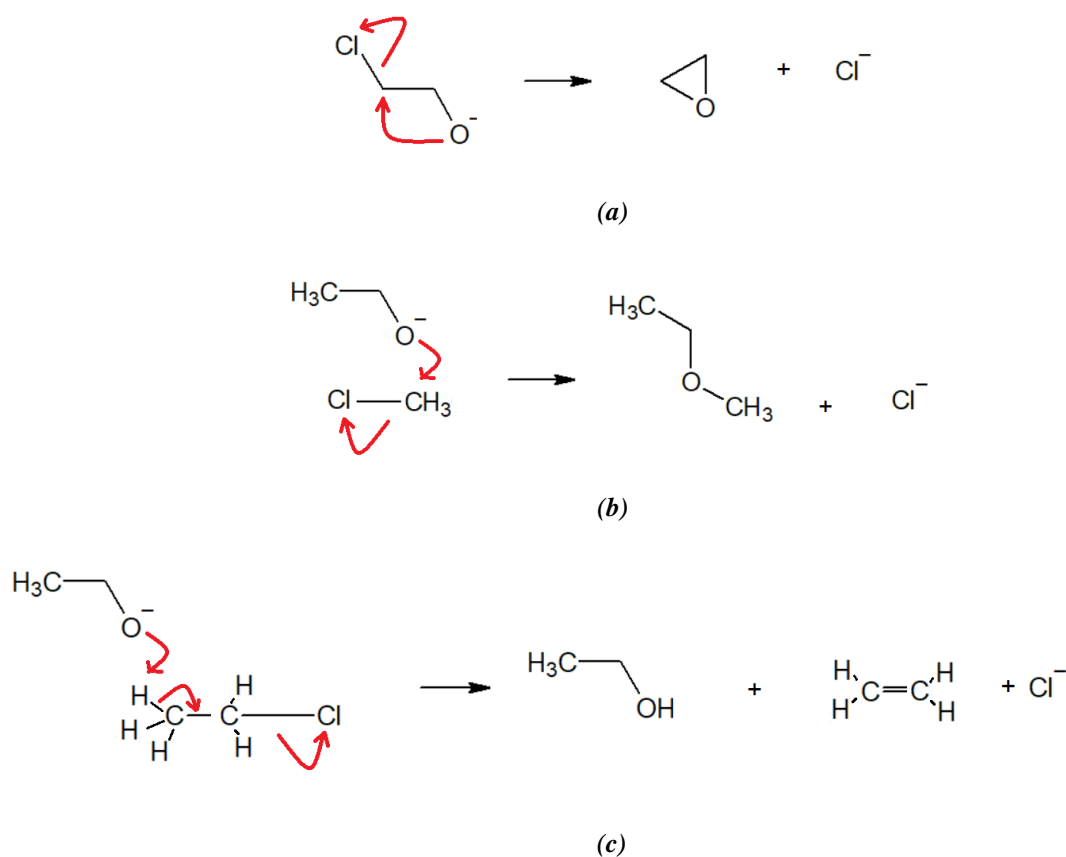


Figure 1. Reactions of alkoxides with halogenated compounds. Intra-molecular synthesis of cyclic ethers (a). Inter-molecular synthesis of linear ethers (b). Alkyl halide elimination (c).

Computational methods

All quantum chemistry computations were performed with the Firefly quantum chemistry package [5], which is partially based on the GAMESS (US) source code [6]. All models were explicitly solvated with seven (or eight) water molecules. The geometries of putative intermediates and transition states in the reaction mechanism were optimized using autogenerated delocalized coordinates [7] using the PBE0 functional [8,9] and the triple-zeta 6-311+G(d,p) basis set. Dispersion effects were accounted for using Grimme's DFT-D3 formalism with Becke-Johnson damping [10]. Zero-point and thermal effects on the free energies at temperatures between 350 K and 500 K were computed at the optimized geometries. Solvation effects were computed using the Polarizable Continuum Model [11-13] implemented in Firefly. Wavefunction analyses and fuzzy bond order computation [14] were performed with Multiwfn 3.8 [15]. Complete geometries of every intermediate described, detailed spreadsheets and full inputs and outputs for all computations have been deposited in Figshare [16].

Results and discussion

The formation of epoxides from halohydrins (Figure 1(a)) was studied first, using 1-chloro-2-propanoxide as the model compound. This model has the halogen in a primary carbon, and additional models with the halogen in a secondary or tertiary carbon were also studied to ascertain both the influence of steric and inductive effects on the reaction outcome. In all cases, seven or eight water molecules solvated the alkoxide moiety to properly mimic the charge dispersion observed in solution. Comparison of the transition state geometries reveals that as the attacked carbon changes from primary to tertiary the transition state distance between attacked carbon and leaving halogen increases noticeably, simultaneous with a decrease of the carbon-chlorine bond order (from 0.52, in the primary transition state to 0.28 in the tertiary transition state) and a smaller decrease in the carbon-oxygen bond order (from 0.66, in the primary transition state to 0.49 in the tertiary transition state). This decrease in bond orders is, however, too small to cause a change in mechanism from S_N2 to S_N1 as the reactants change from a primary to a secondary halohydrin. As expected from an S_N2

reaction, the quantum chemical computations showed that the activation energies increased markedly when moving from a primary to a tertiary carbon (Figure 2). The imaginary frequencies associated with the transition state decrease from 407 i cm^{-1} (primary halohydrin) to 402 i cm^{-1} (secondary halohydrin) and 297 i cm^{-1} (tertiary halohydrin), revealing a pattern where higher activation energies accompany “looser” transition states. Surprisingly, after consideration of all factors (including solvation and vibrational/entropic effects) the attack on a

secondary halogenated carbon proved to be more favourable than the attack on a primary halogenated carbon (Table 1, final columns). Application of Eyring’s equation Eq.(1).

$$\text{rate} = \frac{kT}{h} e^{\frac{-\Delta G^{\text{act}}}{RT}} \quad (1)$$

to the computed activation energies reveals a 5-fold **increase** and 400-fold **decrease** in reaction rate as the reactant is changed from a primary to a secondary, and then to a tertiary halohydrin.

Table 1

| Energetic barriers of the conversion of deprotonated halohydrins into the corresponding epoxides. | | | | |
|--|--|---|---|---|
| | <i>Gas phase ΔE</i> (kJ/mol) | <i>Solution ΔE</i> (kJ/mol) | <i>ΔG (at 350 K)</i> (kJ/mol) | <i>ΔG (at 500 K)</i> (kJ/mol) |
| Primary halohydrin | 71.6 | 61.3 | 60.1 | 60.7 |
| Secondary halohydrin | 90.8 | 71.5 | 55.0 | 44.9 |
| Tertiary halohydrin | 118.4 | 102.2 | 77.5 | 73.3 |

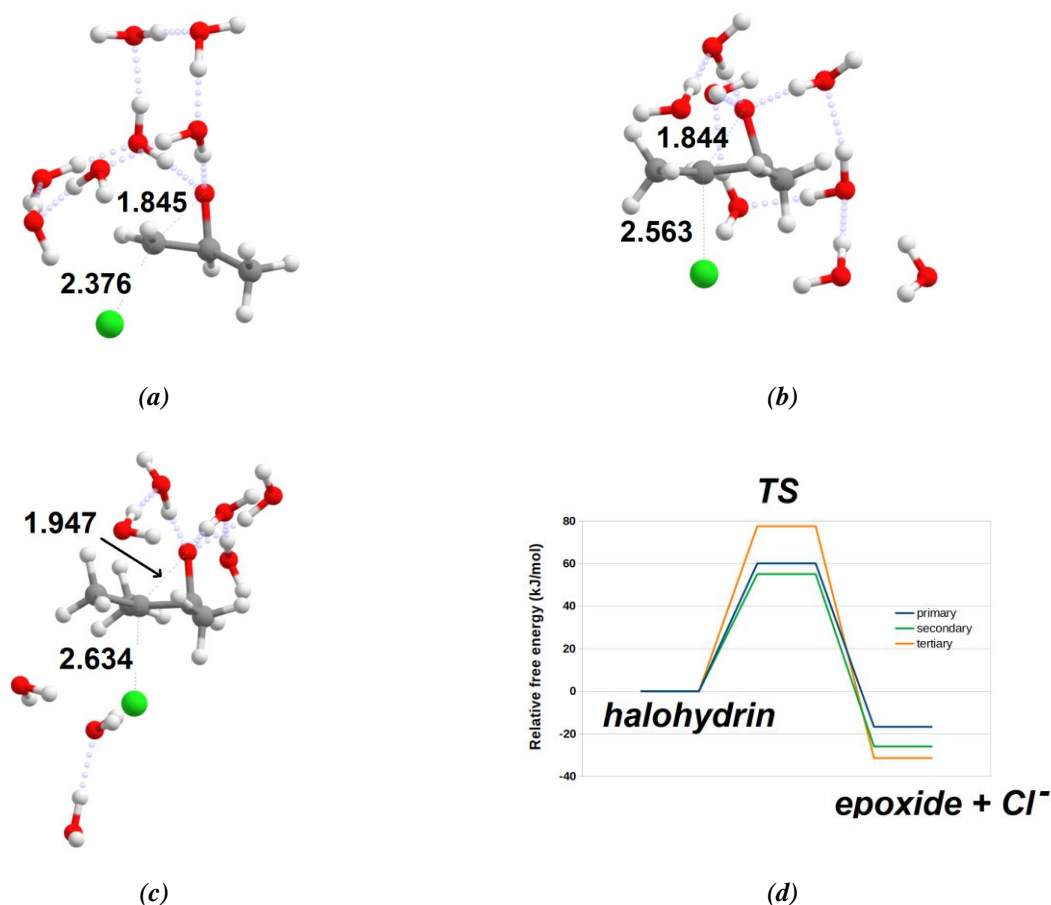


Figure 2. Transition state geometries for the epoxide formation from primary (a), secondary (b) or tertiary halohydrins (c). Potential energy surface at 350 K (d). All energies shown include solvation effects computed with the PCM model. All energies shown include solvation effects computed with the PCM model and ZPVE and vibrational effects at 350 K.

Analysis of the different energetic contributions to this phenomenon shows that the increased reactivity of the secondary halohydrin is completely due to vibrational/entropic effects: when those effects are neglected, the expected monotonous trend in activation energies is found, rising from relatively low values (61.3 kJ/mol, for a primary halohydrin) to 71.5 kJ/mol (for a secondary halohydrin), and thence to an elevated 102.2 kJ/mol barrier (for the attack on the tertiary halohydrin). The resulting epoxides are more stable than the reactants, largely due to the favourable contribution of product solvation and to the increase in vibrational entropy afforded by the replacement of a C-Cl bond by a novel ether bond, which is especially noticeable in the more substituted ethers (Table 2). These combined effects explain why the reaction proceeds in the direction of epoxide formation despite the strained nature of the resulting product.

Additional computations (Tables 3 and 4, Figure 3) show that the attack of the resulting epoxide by small excesses of hydroxide in the reaction mixture are unlikely to perturb the experimental outcome dramatically: although this attack is thermodynamically quite favoured, this alternative reaction has substantially higher activation energy than the putative attack by Cl⁻, which entails a 230-fold lower reaction rate and prevents this side-reaction from destroying the formed epoxide unless the concentration of hydroxide is several orders of magnitude higher than that of the epoxide.

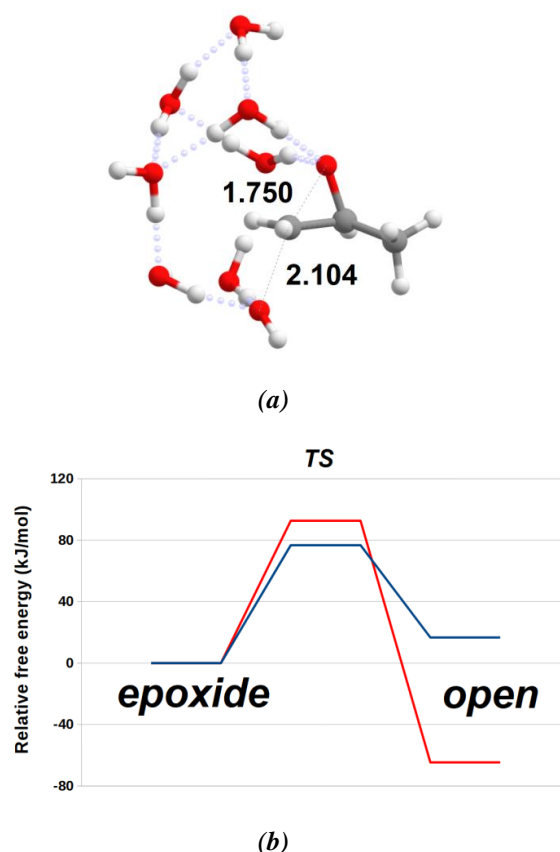


Figure 3. Transition state geometry for the opening reaction of a primary epoxide using HO⁻ (a). Potential energy surfaces for epoxide opening using Cl⁻ (blue trace) or HO⁻ (red trace) at 350 K (b). All energies shown include solvation effects computed with the PCM model and ZPVE and vibrational effects at 350 K.

Table 2

| Reaction energies of the conversion of deprotonated halohydrins into the corresponding epoxides. | | | | |
|---|--|---|-----------------------------------|-----------------------------------|
| | <i>Gas phase ΔE</i> (kJ/mol) | <i>Solution ΔE</i> (kJ/mol) | ΔG (at 350 K) (kJ/mol) | ΔG (at 500 K) (kJ/mol) |
| Primary halohydrin | 8.5 | -12.2 | -16.7 | -20.1 |
| Secondary halohydrin | -21.9 | -17.0 | -25.9 | -39.5 |
| Tertiary halohydrin | 26.1 | -0.3 | -31.4 | -46.0 |

Table 3

| Energetic barriers of the epoxide opening upon nucleophilic attack. | | | | |
|--|--|---|-----------------------------------|-----------------------------------|
| <i>Nucleophile:</i> | <i>Gas phase ΔE</i> (kJ/mol) | <i>Solution ΔE</i> (kJ/mol) | ΔG (at 350 K) (kJ/mol) | ΔG (at 500 K) (kJ/mol) |
| Cl ⁻ | 63.1 | 73.6 | 76.7 | 77.5 |
| HO ⁻ | 87.9 | 82.7 | 92.6 | 98.1 |

Table 4

| Reaction energies of the epoxide opening upon nucleophilic attack. | | | | |
|---|--|---|-----------------------------------|-----------------------------------|
| <i>Nucleophile:</i> | <i>Gas phase ΔE</i> (kJ/mol) | <i>Solution ΔE</i> (kJ/mol) | ΔG (at 350 K) (kJ/mol) | ΔG (at 500 K) (kJ/mol) |
| Cl ⁻ | -8.5 | 12.2 | 16.7 | 20.1 |
| HO ⁻ | -74.4 | -79.3 | -64.7 | -60.0 |

The thermodynamic differences between the epoxide attack by Cl^- (endergonic by 16.7 kJ/mol) and HO^- (exergonic by 64.7 kJ/mol) can largely (though not only) be explained by the difference in bond dissociation enthalpies [17] of C-Cl (≈ 350 kJ/mol) and C-OH (≈ 385 kJ/mol) bonds.

To ascertain more precisely how the cost of producing a strained epoxide affected the kinetics and thermodynamics of these intramolecular Williamson's ether synthesis, the formation of cyclic ethers with progressively larger rings (and, accordingly, less angular strain) was studied next. Geometrically, the transition states leading to the larger rings consistently showed longer C-O bonds and shorter C-Cl bonds than the corresponding transition state leading to the epoxide (compare Figure 4 and 3(a)). As expected, the computations confirmed (Figure 4(d) and Table 6) that the reaction became progressively more exergonic as the ring size increased to 5 atoms, when ring strain mostly vanishes, but no clear trend in activation energy (Figure 5) could be discerned as the ring size grew. Surprisingly, electronic energy barriers increased as the ring grew, and a decrease (consistent with intuitive expectation) was only observed for a ring size of five. Solvation effects slightly facilitate the formation of the transition state leading to all cyclic ethers, whereas vibrational/entropic effects disfavour the formation of the 4-atom oxetane ring. When considering all effects, the activation energy for the formation of the six-atom 1-methyl-tetrahydropyran ring is barely distinguishable from that of the much more strained epoxide ring, whereas the formation of the 4-atom oxetane ring has an activation energy 26 kJ/mol above that of

the epoxide, and the activation energy of the reaction leading to the five-atom 1-methyl-tetrahydrofuran ring was around 19 kJ/mol lower than the one leading to the comparably strain-free 1-methyl-tetrahydropyran ring (Tables 5 and 6). The reaction rates that can be computed from these activation energies using Eyring's equation follow the trend tetrahydrofuran>epoxide>tetrahydropyran>oxetane, and span five orders of magnitude. In these syntheses of cyclic ethers through attack of alkoxides on primary carbon atoms, the imaginary frequencies associated with the transition state consistently fall in a relatively narrow interval (from 394 i cm^{-1} to 482 i cm^{-1}). In the gas-phase, the activation energy of these reactions and the frequency of the vibration associated with the transition state increase in perfect lockstep.

The experimentally observed trend for the reaction rates of cyclic ether formation (epoxide>tetrahydrofuran>tetrahydropyran>oxetane [4]) has previously been explained by invoking both the increased ring strain in epoxide and oxetane and the increase of conformational flexibility (and therefore conformational entropy) as the halogenated carbon is placed an increased number of C-C bonds away from the deprotonated alkoxide function. The computations above show that the relative ordering of the reaction rates for rings between 4 and 6 can, in contrast, be explained without invoking those factors, and that the preference for tetrahydrofuran over tetrahydropyran formation is instead due to a hitherto unsuspected high activation energy of the pathway leading to the strain-free tetrahydropyran.

Table 5

Energetic barriers of the conversion of other deprotonated chloroalkane alcohols into the corresponding epoxides.

| <i>Cyclic ether product:</i> | <i>Gas phase ΔE</i> (kJ/mol) | <i>Solution ΔE</i> (kJ/mol) | <i>ΔG (at 350 K)</i> (kJ/mol) | <i>ΔG (at 500 K)</i> (kJ/mol) |
|------------------------------|--|---|---|---|
| Epoxide | 71.6 | 61.3 | 60.1 | 60.7 |
| Oxetane | 82.1 | 72.6 | 86.1 | 98.6 |
| 1-Methyl-tetrahydrofuran | 52.9 | 55.5 | 55.6 | 58.5 |
| 1-Methyl-tetrahydropyran | 76.0 | 83.2 | 74.8 | 72.5 |

Table 6

Reaction energies of the conversion of other deprotonated chloroalkane alcohols into the corresponding epoxides.

| <i>Cyclic ether product:</i> | <i>Gas phase ΔE</i> (kJ/mol) | <i>Solution ΔE</i> (kJ/mol) | <i>ΔG (at 350 K)</i> (kJ/mol) | <i>ΔG (at 500 K)</i> (kJ/mol) |
|------------------------------|--|---|---|---|
| Epoxide | 8.5 | -12.2 | -16.7 | -20.1 |
| Oxetane | -5.6 | -38.6 | -35.3 | -35.0 |
| 1-Methyl-tetrahydrofuran | -92.0 | -111.5 | -109.8 | -111.4 |
| 1-Methyl-tetrahydropyran | -76.8 | -84.3 | -85.5 | -90.1 |

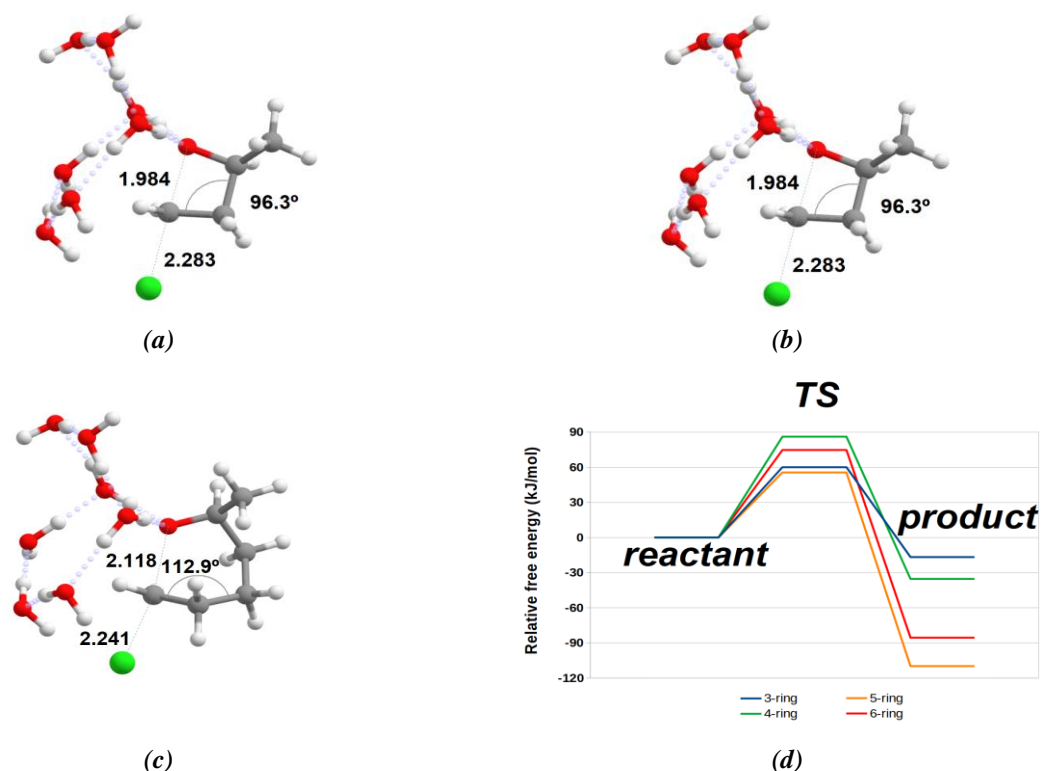


Figure 4. Transition state geometry for formation of cyclic ethers with 4 ring atoms (oxetane) (a), 5 ring atoms (1-methyl-tetrahydrofuran) (b), and 6 ring atoms (1-methyl-tetrahydropyran) (c). Potential energy surfaces for the formation of epoxide, oxetane, 1-methyl-tetrahydrofuran, and 1-methyl-tetrahydropyran rings from the corresponding halogenated alkoxides at 350 K (d). All energies shown include solvation effects computed with the PCM model and ZPVE and vibrational effects at 350 K.

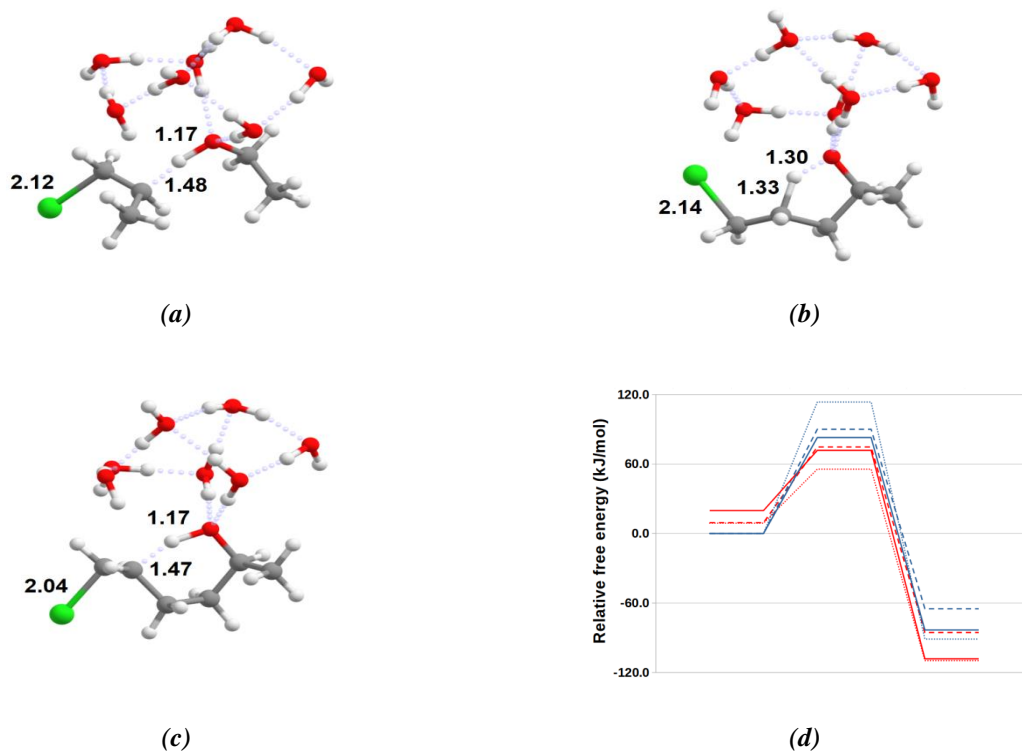


Figure 5. Transition state geometry for competing elimination reactions in the attempted synthesis of ethylpropyl ether (a), 1-methyl-tetrahydrofuran (b), and 1-methyl-tetrahydropyran (c). The potential energy surfaces of ether synthesis (red) and elimination reactions (blue) of 5-chloro-2-pentanoxide (dotted lines), 6-chloro-2-hexanoxide (broken lines), and ethoxide+1-chloropropane (full lines) at 350 K (d). All energies shown include solvation effects computed with the PCM model and ZPVE and vibrational effects at 350 K.

Although the analyses of the transition state geometries do not reveal any obvious reason for such a surprising behaviour, an inspection of the initial reactant states shows that two factors contribute to the lower reaction rate of the tetrahydropyran formation: first, the preference for the successive $-\text{CH}_2-$ units in the reactant to adopt staggered conformations relative to their neighbours leads the reacting CH_2Cl moiety in the 6-chloro-2-hexanoxide that leads to the 1-methyl-tetrahydropyran (unlike the one in the 5-chloro-2-pentanoxide that leads to the 1-methyl-tetrahydrofuran) to adopt a position where an additional partial rotation is required before it is geometrically aligned to allow attack by the alkoxide. Additionally, in the reactant state, the distance between the alkoxide moiety and the halogenated carbon is also observed to be larger (3.12 Å) in the 6-chloro-2-hexanoxide leading to the six-atom ring than in the 5-chloro-2-pentanoxide (2.93 Å) that yields the five-atom ring.

While successful in explaining most of the experimental results, the computations above do not yet agree with the experimental observations establishing that the formation of the small epoxide ring is faster than that of tetrahydrofuran. Whether the discrepancy is due to an over-prediction of the activation energy for the formation of the epoxide or the under-prediction of the activation energy of tetrahydrofuran synthesis remains to be ascertained.

Synthesis of linear (instead of cyclic) ethers through this reaction (Figure 1(b)) may naturally

be expected to be governed by somewhat different factors: for example, in the linear case the two reactive moieties are present in two independent molecules, which entails that the reaction might not be as susceptible to the geometric constraints that decrease reaction rate in the larger cyclic cases described above; on the other hand, the reaction exergonicity may be predicted to not benefit as much from entropic effects since no change in molecularity occurs between reactants and products. Interestingly, the results of the computation of the reaction pathway for the synthesis of ethyl-propyl ether from deprotonated ethoxide and 1-chloropropane (Table 7) reveal that, while the separated reactants indeed do not suffer from the unfavourable geometric penalties observed in the syntheses of oxetane or 1-methyl-tetrahydropyran, they are nonetheless less favourable than those observed in the synthesis of the cyclic 1-methyl-tetrahydrofuran: the internal reaction of 5-chloro-2-pentanoxide is favoured relative to that of the separated reactants because a much smaller entropic penalty is incurred when approaching the two reacting moieties when they are present in the same molecule.

The intervention of a strong base (alkoxide) in this reaction leads to the possibility of an unfavourable competition with an elimination reaction (Figure 1(c)) when the haloalkane contains hydrogens at the β -position. In all cases studied (Figure 5 and Table 8), the elimination reactions have higher activation energies than the ether syntheses at 350 K.

Table 7

Relative energies of transition state and product in the Williamson's synthesis of ethylpropyl ether from ethoxide and 1-chloropropane.

| | Gas phase ΔE (kJ/mol) | Solution ΔE (kJ/mol) | ΔG (at 350 K) (kJ/mol) | ΔG (at 500 K) (kJ/mol) |
|------------------|----------------------------------|---------------------------------|-----------------------------------|-----------------------------------|
| Transition state | 71.6 | 60.3 | 71.8 | 75.5 |
| Product | -76.0 | -119.4 | -108.2 | -109.0 |

Table 8

Relative energies of transition states and products of alkoxide-promoted elimination reactions.

| | Gas phase ΔE (kJ/mol) | Solution ΔE (kJ/mol) | ΔG (at 350 K) (kJ/mol) | ΔG (at 500 K) (kJ/mol) |
|-----------------------------------|----------------------------------|---------------------------------|-----------------------------------|-----------------------------------|
| Ethoxide+1-chloropropane (TS) | 111.5 | 96.3 | 82.8 | 80.9 |
| Ethanol+1-propene + Cl^- | -62.5 | -78.7 | -83.2 | -87.1 |
| 5-Chloro-2-pentanoxide (TS) | 108.7 | 122.0 | 113.5 | 114.9 |
| 4-Penten-2-ol + Cl^- | -98.0 | -93.5 | -91.1 | -90.6 |
| 6-Chloro-2-hexanoxide (TS) | 108.0 | 101.5 | 90.0 | 90.2 |
| 5-Penten-2-ol + Cl^- | -62.1 | -69.2 | -65.0 | -62.5 |

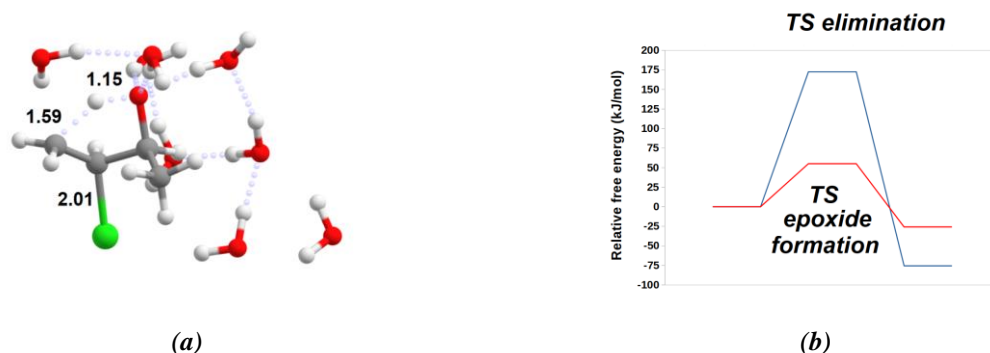


Figure 6. Transition state geometry for the elimination reaction in the attempted epoxide synthesis from a secondary halohydrin (a). The potential energy surfaces of ether synthesis (red) and elimination reaction (blue) at 350 K (b). All energies shown include solvation effects computed with the PCM model and ZPVE and vibrational effects at 350 K.

Whereas the elimination does not suffer from steric penalties when the reacting moieties are borne by different molecules (Figure 5(a)), comparison of the transition states of the elimination reactions of 1-chloropropane, 5-chloro-2-pentanoxide and 6-chloro-2-hexanoxide reveals that the geometry of the elimination is extremely strained in the reactions of 5-chloro-2-pentanoxide (the reactant that can otherwise lead to 1-methyl-tetrahydrofuran) or, and hardly any geometric strain seems to exist in the reactant that leads to 1-methyl-tetrahydropyran (6-chloro-2-hexanoxide). As a consequence, the elimination reaction does not compete at all with intramolecular cyclic ether synthesis from 5-chloro-2-pentanoxide (Figure 5(d), Tables 5 and 8), but it may compete to a small extent in the case of 6-chloro-hexanoxide, due to the smaller gap between activation energies of the two pathways in the latter case. In contrast to the ether syntheses reactions (Tables 1, 3, 5, and 7), whose activation energies usually increase with temperature, the activation energy of the intermolecular elimination reaction decreases with temperature (Table 8). This dependence of activation free energy with temperature entails that increasing the temperature benefits the inter-molecular elimination reaction rate *vs.* that of the inter-molecular ether synthesis, leading to a preference for elimination at higher temperatures, as is well-known experimentally [1]. These reaction rates have the opposite temperature dependence in the 6-chloro-2-hexanoxide case, which is therefore predicted (like 5-chloro-2-pentanoxide) to always afford significantly lower activation energies for the pathway leading to the cyclic ether

(1-methyl-tetrahydropyran) than for the elimination pathway.

The unfavourable steric effects observed in the elimination reaction of 5-chloro-2-propanoxide are present, to a somewhat larger degree, when the alkoxide attempts to capture hydrogen from a methyl group adjacent to the halogenated carbon in a secondary halohydrin (Figure 6).

The increased difficulty can be attributed to the unfavourable orbital geometry around the halogenated carbon because its bonds to both the C_β and to the alkoxide carbon atom prevent it from adopting the quasi-planar conformation needed for a proper overlap between the occupied *p*-orbital on C_β and the empty orbital that has been left on C_α due to the heterolytic breaking of the C-Cl bond.

Conclusions

The density functional theory computations described above afford the answers to several issues thus far unanalysed in the literature. It can be concluded that epoxide generation from halohydrins is achieved, despite the considerable ring strain in the products, through the combined effects of favourable solvation of the products, higher bond enthalpy of the formed C-O bond *vs.* the broken C-Cl bond, and through increased vibrational entropy of the epoxide *vs.* the original halohydrin. The vibrational effects are shown to be especially important in the more highly substituted epoxides, where they can become responsible for as much as 30 kJ/mol of extra stabilization. Competing elimination reactions during epoxide synthesis, which might be expected to occur when a methyl substituent is

present on the halogenated carbon, are prevented due to steric effects that oppose the halogenated carbon from approaching the quasi-planar geometries needed for the formation of a C=C double bond.

The rates of formation of larger cyclic ethers are here shown to depend mostly on geometric factors, and to be suitably explained without the need to invoke increases in conformational entropy as additional methylene units are placed between the reacting alkoxide and halogenated carbon. Instead, the decreased formation rate of the six-atom cyclic ether vs. the five-atom cyclic ether is due to the larger initial distance between the reacting moieties in the reactant conformation, and especially to the unfavourable alignment of the C-Cl bond vs. the direction of attack of the alkoxide. Elimination reactions do not compete with the formation of these cyclic ethers due to unfavourable geometry, which is especially noticeable in the reaction leading to the five-atom cyclic ether. Elimination does not suffer from geometric penalties when the reacting moieties are present in different molecules, which enables it to compete with the synthesis of linear ethers, especially at higher temperatures. This temperature dependence is a consequence of a peculiar increase of activation entropy with temperature of the elimination pathway, which contrasts with the predicted decrease in activation entropy of the linear ether synthesis as the temperature rises.

References

- Carey, F.A. *Organic Chemistry*. McGraw-Hill Higher Education: New York, 2000, 1275 p.
- Solomons, T.W.G.; Fryhle, C.B. *Organic Chemistry*. John Wiley & Sons: New York, 2000, 1344 p.
- Wang, Z. "Williamson Ether Synthesis". *Comprehensive Organic Name Reactions and Reagents*. John Wiley & Sons: New York, 2010, pp. 3026–3030. DOI: <https://doi.org/10.1002/9780470638859.conrr673>
- Ouellette, R.J.; Rawn, J.D. Ethers and Epoxides. *Organic Chemistry*, 2014, pp. 535–565. DOI: <https://doi.org/10.1016/B978-0-12-800780-8.00016-4>
- Granovsky, A.A. Firefly computational chemistry program. Firefly 8.0.0. 2013. <http://classic.chem.msu.su/gran/gamess/index.html>
- Schmidt, M.W.; Baldrige, K.K.; Boatz, J.A.; Elbert, S.T.; Gordon, M.S.; Jensen, J.H.; Koseki, S.; Matsunaga, N.; Nguyen, K.A.; Su, S.; Windus, T.L.; Dupuis, M.; Montgomery, J.A. General atomic and molecular electronic structure system. *Journal of Computational Chemistry*, 1993, 14(11), pp. 1347–1363. DOI: <https://doi.org/10.1002/jcc.540141112>
- Baker, J.; Kessi, A.; Delley, B. The generation and use of delocalized internal coordinates in geometry optimization. *The Journal of Chemical Physics*, 1996, 105(1), pp. 192–212. DOI: <https://doi.org/10.1063/1.471864>
- Adamo, C.; Barone, V. Toward reliable density functional methods without adjustable parameters: The PBE0 model. *The Journal of Chemical Physics*, 1999, 110(13), pp. 6158–6170. DOI: <https://doi.org/10.1063/1.478522>
- Ernzerhof, M.; Scuseria, G.E. Assessment of the Perdew–Burke–Ernzerhof exchange–correlation functional. *The Journal of Chemical Physics*, 1999, 110(11), pp. 5029–5036. DOI: <https://doi.org/10.1063/1.478401>
- Grimme, S.; Ehrlich, S.; Goerigk, L. Effect of the damping function in dispersion corrected density functional theory. *Journal of Computational Chemistry*, 2011, 32(7), pp. 1456–1465. DOI: <https://doi.org/10.1002/jcc.21759>
- Tomasi, J.; Persico, M. Molecular interactions in solution: An overview of methods based on continuous distributions of the solvent. *Chemical Reviews*, 1994, 94(7), pp. 2027–2094. DOI: <https://doi.org/10.1021/cr00031a013>
- Cossi, M.; Mennucci, B.; Pitarch, J.; Tomasi, J. Correction of cavity-induced errors in polarization charges of continuum solvation models. *Journal of Computational Chemistry*, 1998, 19(8), pp. 833–846. DOI: [https://doi.org/10.1002/\(sici\)1096-987x\(199806\)19:8<833::aid-jcc3>3.0.co;2-q](https://doi.org/10.1002/(sici)1096-987x(199806)19:8<833::aid-jcc3>3.0.co;2-q)
- Mennucci, B.; Tomasi, J. Continuum solvation models: A new approach to the problem of solute's charge distribution and cavity boundaries. *The Journal of Chemical Physics*, 1997, 106(12), pp. 5151–5158. DOI: <https://doi.org/10.1063/1.473558>
- Mayer, I.; Salvador, P. Overlap populations, bond orders and valences for 'fuzzy' atoms. *Chemical Physics Letters*, 2004, 383(3–4), pp. 368–375. DOI: <https://doi.org/10.1016/j.cplett.2003.11.048>
- Lu, T.; Chen, F. Multiwfn: A multifunctional wavefunction analyzer. *Journal of Computational Chemistry*, 2012, 33(5), pp. 580–592. DOI: <https://doi.org/10.1002/jcc.22885>
- Silva, P.J. Computational exploration of Williamson's method for ether (and epoxide) synthesis. Figshare Dataset, 2023. DOI: <https://doi.org/10.6084/m9.figshare.22787492.v2>
- Luo, Y.-R. *Comprehensive Handbook of Chemical Bond Energies*. CRC Press: New York, 2007, 1688 p. DOI: <https://doi.org/10.1201/9781420007282>